

# Elastocaloric response of $\text{PbTiO}_3$ predicted from a first-principles effective Hamiltonian

J. A. Barr and S. P. Beckman

*Department of Materials Science and Engineering, Iowa State University, Ames, Iowa 50011*

Takeshi Nishimatsu

*Institute for Materials Research (IMR), Tohoku University, Sendai 980-8577, Japan*

A first-principles based effective Hamiltonian is used within a molecular dynamics simulation to study the elastocaloric effect in  $\text{PbTiO}_3$ . It is found that the transition temperature is a linear function of uniaxial tensile stress. Negative temperature change is calculated, when the uniaxial tensile stress is switched off, as a function of initial temperature  $\Delta T(T_{\text{initial}})$ . It is predicted that the formation of domain structures under uniaxial tensile stress degrades the effectiveness of the elastocaloric effect.

PACS numbers: 64.60.De, 77.80.B-, 77.84.-s

## I. INTRODUCTION

Solid-state caloric effects provide a promising approach to future refrigeration technologies. The electrocaloric<sup>1–4</sup>, magnetocaloric<sup>5,6</sup>, and barocaloric effects<sup>7,8</sup> produce a temperature change due to entropic changes induced by the application of an electric field, magnetic field, and pressure, respectively. The application of a uniaxial stress to a ferroelectric material affects the spontaneous polarization and produces an adiabatic temperature change. This is called the elastocaloric effect<sup>9–13</sup>.

Here, a first-principles effective Hamiltonian model implemented within a molecular dynamics (MD) framework, is used to predict the elastocaloric response of  $\text{PbTiO}_3$ . Following the work of Lisenkov *et al.* in Ref. 11, the elastocaloric response of  $\text{PbTiO}_3$  is examined for tensile uniaxial loads ranging from 0 to  $-2.0$  GPa and temperatures ranging from 300 to 1000 K. These results will be compared to those reported in the literature.

## II. METHODS

The effective Hamiltonian used is

$$\begin{aligned}
 H^{\text{eff}} = & \frac{M_{\text{dipole}}^*}{2} \sum_{\mathbf{R}, \alpha} \dot{u}_{\alpha}^2(\mathbf{R}) + \frac{M_{\text{acoustic}}^*}{2} \sum_{\mathbf{R}, \alpha} \dot{w}_{\alpha}^2(\mathbf{R}) \\
 & + V^{\text{self}}(\{\mathbf{u}\}) + V^{\text{dpl}}(\{\mathbf{u}\}) + V^{\text{short}}(\{\mathbf{u}\}) \\
 & + V^{\text{elas, homo}}(\eta_1, \dots, \eta_6) + V^{\text{elas, inho}}(\{\mathbf{w}\}) \\
 & + V^{\text{coup, homo}}(\{\mathbf{u}\}, \eta_1, \dots, \eta_6) + V^{\text{coup, inho}}(\{\mathbf{u}\}, \{\mathbf{w}\}).
 \end{aligned} \tag{1}$$

Here, the collective atomic motion is coarse-grained by local soft mode vectors  $\mathbf{u}(\mathbf{R})$  and local acoustic displacement vectors  $\mathbf{w}(\mathbf{R})$  of each unit cell at  $\mathbf{R}$  in a simulation supercell.  $\eta_1, \dots, \eta_6$  are six components of homogeneous strain in Voigt notation.  $\frac{M_{\text{dipole}}^*}{2} \sum_{\mathbf{R}, \alpha} \dot{u}_{\alpha}^2(\mathbf{R})$  and  $\frac{M_{\text{acoustic}}^*}{2} \sum_{\mathbf{R}, \alpha} \dot{w}_{\alpha}^2(\mathbf{R})$  are the

kinetic energies possessed by the local soft modes and the local acoustic displacement vectors along with their effective masses of  $M_{\text{dipole}}^*$  and  $M_{\text{acoustic}}^*$ ,  $V^{\text{self}}(\{\mathbf{u}\})$  is the local mode self energy,  $V^{\text{dpl}}(\{\mathbf{u}\})$  is the long-ranged dipole-dipole interaction,  $V^{\text{short}}(\{\mathbf{u}\})$  is the short-ranged interaction between local soft modes,  $V^{\text{elas, homo}}(\eta_1, \dots, \eta_6)$  is the elastic energy from homogeneous strains,  $V^{\text{elas, inho}}(\{\mathbf{w}\})$  is the elastic energy from inhomogeneous strains,  $V^{\text{coup, homo}}(\{\mathbf{u}\}, \eta_1, \dots, \eta_6)$  is the coupling between the local soft modes and the homogeneous strain, and  $V^{\text{coup, inho}}(\{\mathbf{u}\}, \{\mathbf{w}\})$  is the coupling between the soft modes and the inhomogeneous strains. Details of this Hamiltonian are explained in Refs. 14–16. Additionally, to investigate effects from stress, we use enthalpy  $\mathcal{H} = H^{\text{eff}} + Na_0^3 \boldsymbol{\sigma} \cdot \boldsymbol{\eta}$ , where  $N = L_x \times L_y \times L_z$  is the supercell size,  $a_0$  is the unit cell length, therefore  $Na_0^3$  is the supercell volume, and  $\boldsymbol{\sigma}$  is the six components of stress. In this study, we apply uniaxial tensile stress to the system along the  $z$  direction. It is implemented in the MD framework and the MD simulation program is called **feram**. **feram** is distributed as free software under the conditions described in the GNU General Public License from its website <http://loto.sourceforge.net/feram/>. Examples of the input files are packaged within the source code under the **feram-0.22.04/src/28example-PbTiO3-elastocaloric-770K/** directory. The model parameters for  $\text{PbTiO}_3$  are determined semi-empirically in earlier work<sup>17</sup> and adopted for **feram** in Ref. 18.

As shown in Fig. 1, the simulation procedure for determining the elastocaloric response of  $\text{PbTiO}_3$  is similar to that used for the “direct” prediction of the electrocaloric effect presented in Ref. 19. A supercell size of  $N = 64 \times 64 \times 64$  is used and is thermalized for 50,000 times steps in a canonical ensemble at constant initial temperature,  $T_{\text{initial}}$ , and constant applied stress. A single-domain  $+z$ -polarized initial configuration for the first thermalization MD is generated randomly with certain averages and deviations for  $\{\mathbf{u}\}$ :  $\langle u_x \rangle = \langle u_y \rangle = 0$ ,  $\langle u_z \rangle = 0.33 \text{ \AA}$ ,  $\langle u_x^2 \rangle - \langle u_x \rangle^2 = \langle u_y^2 \rangle - \langle u_y \rangle^2 = (0.045 \text{ \AA})^2$ ,

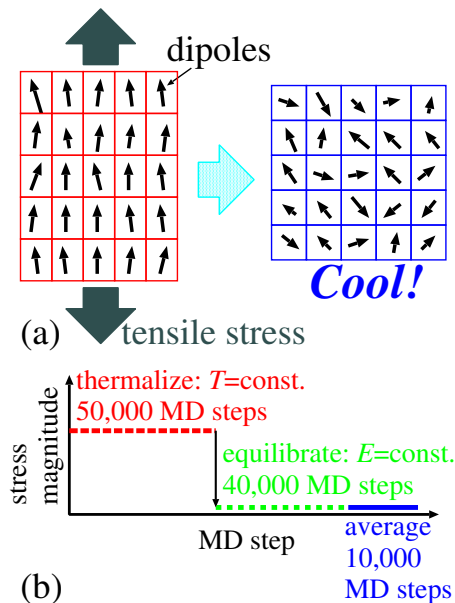


FIG. 1. (Color online) (a) Schematic illustration of elastocaloric cooling. (b) Procedure of direct simulation of the elastocaloric effect.

and  $\langle u_z^2 \rangle - \langle u_z \rangle^2 = (0.021 \text{ \AA})^2$ . Once thermalized, the system is switched from being held at constant temperature to being isolated as a microcanonical ensemble. The mechanical load is removed and the system is allowed to equilibrate for 40,000 time steps. Once equilibrated, the system's final temperature,  $T_{\text{final}}$ , is determined by averaging the acoustic and dipole kinetic energies for 10,000 time steps. The time step for this simulation is 2 fs. The temperature ranges from 300 to 1000 K, incremented with a step size of 1 K, and the applied uniaxial stress ranges from 0 to  $-2.0$  GPa, incremented with a step size of  $-0.2$  GPa.

### III. RESULTS AND DISCUSSION

The elastocaloric response,  $\Delta T_{\text{raw}} = T_{\text{final}} - T_{\text{initial}}$ , of  $\text{PbTiO}_3$  is presented in Fig. 2(a). Scaling from  $\Delta T_{\text{raw}}$  to  $\Delta T_{\text{corrected}} = \frac{2}{5} \Delta T_{\text{raw}}$  must be employed to account for the reduced degrees of freedom due to coarse-graining as discussed in Ref. 19. In Fig. 2(b), polarizations along the  $z$  direction for before and after the release of the load of  $\sigma_3 = -1.6$  GPa are compared, i.e.  $P_z(T_{\text{initial}}, \sigma_3 = -1.6 \text{ GPa})$  and  $P_z(T_{\text{final}}, \sigma_3 = 0)$  are compared, respectively. We redefine the transition temperature under uniaxial stress as  $T'_C(\sigma_3)$ . For  $\sigma_3 = -1.6$  GPa,  $T'_C = 917$  K. Transformation from  $T'_C$  is indicated with a dashed blue arrow. Above a certain temperature,  $T_{\text{onset}}$ , there is a temperature range  $T_{\text{onset}} < T_{\text{initial}} \leq T'_C$  in which one can get a large elastocaloric effect. Transformation from  $T_{\text{onset}}$  is indicated with a dotted magenta arrow. It can be seen that below  $T_{\text{onset}}$  ( $T_{\text{initial}} \leq T_{\text{onset}}$ ), transformation from switching off the uniaxial tensile stress is from an

elongated ferroelectric polarized state to a normal ferroelectric polarized state. Between  $T_{\text{onset}}$  and  $T'_C$ , i.e.  $T_{\text{onset}} < T_{\text{initial}} \leq T'_C$ , the transformation changes from a stress-enhanced ferroelectric polarized state to a paraelectric non-polar state, resulting in a large elastocaloric response. Just above  $T_{\text{onset}}$  occurs a maximum  $|\Delta T|$  and its transformation is indicated with a solid red arrow, in Fig. 2(b). Above  $T'_C$  ( $T'_C < T_{\text{initial}}$ ), even under the uniaxial tensile stress load, the system remains paraelectric and consequently  $|\Delta T| = 0$ .

In Fig. 2(c)–(e),  $P_z(T_{\text{initial}}, \sigma_3 \leq 0)$  and  $P_z(T_{\text{final}}, \sigma_3 = 0)$  are plotted also for loads of  $\sigma_3 = -0.8, -0.4$  and  $0.0$  GPa. In Fig. 2(c), it is observed that with a load of  $-0.8$  GPa, the effective temperature range  $T_{\text{onset}} < T_{\text{initial}} \leq T'_C$  becomes narrower compared to that of  $-1.6$  GPa. In Fig. 2(d), it can be seen that the initial uniaxial tensile load of  $-0.4$  GPa is not large enough to induce a ferroelectric-to-paraelectric transformation. Therefore, we cannot define  $T_{\text{onset}}$  for loads of  $0.0 < \sigma_3 < -0.4$  GPa. With  $0.0$  GPa load, in Fig. 2(e), accuracy of our MD simulations ( $\Delta T \equiv 0$ ) and the simulated phase transition temperature of  $T_C = 640$  K under zero pressure are shown. This value is in good agreement with the earlier Monte Carlo<sup>17</sup> and MD<sup>18</sup> simulations, in which the same set of parameters were used, and is slightly lower than the experimental value  $T'_C(0) = T_C = 763$  K.

As anticipated, the greater the uniaxial loading, the greater the induced temperature change,  $|\Delta T|$ , and for a loading of  $-2.0$  GPa a temperature change of  $-43$  K is predicted.

In Fig. 3, plots show  $\max|\Delta T_{\text{corrected}}|$ , and  $T_{\text{onset}}$  and  $T'_C$  under different applied loads. It can be seen that  $T'_C$  depends on applied load linearly.  $T_{\text{onset}}$  depends on applied load nearly linearly in  $-0.6 < \sigma_3 < -2.0$ , but less steeply compared to  $T'_C$ .

$T_{\text{onset}}$  is also found to depend on the period of equilibration. Between  $T_C$  and  $T_{\text{onset}}$  ( $T_C < T_{\text{initial}} \leq T_{\text{onset}}$ ), when a uniaxial tensile stress is applied and then released, the system stays in a ferroelectric state and does not transform into a paraelectric state. In other words, the system *remembers* the strength of the stress applied. This is confirmed with longer equilibration of 990,000 time steps instead of the 40,000 in Fig. 1. As shown with black chain lines in Figs. 2(a) and (c),  $T_{\text{onset}}$  with longer equilibration becomes 736 K, while 40,000's was 744 K, i.e. the system *forgets* the strength of the stress applied. Therefore, the stronger load and the shorter period of equilibration results in the higher  $T_{\text{onset}}$ .

Contrarily, in Fig. 4, we also perform “heating” simulations with switching-on of uniaxial stress in which system is firstly thermalized under zero stress and then  $\Delta T$  is measured under switched-on uniaxial tensile stresses. Zigzag structures in final temperatures are observed. A cross section and a slice of a final state indicated with a “+” mark in Fig. 4 are shown in Figs. 5 and 6, respectively. The supercell is divided into  $+z$  and  $-z$  domains. It can be understood that the zigzag structures are coming from existence and non-existence of domain

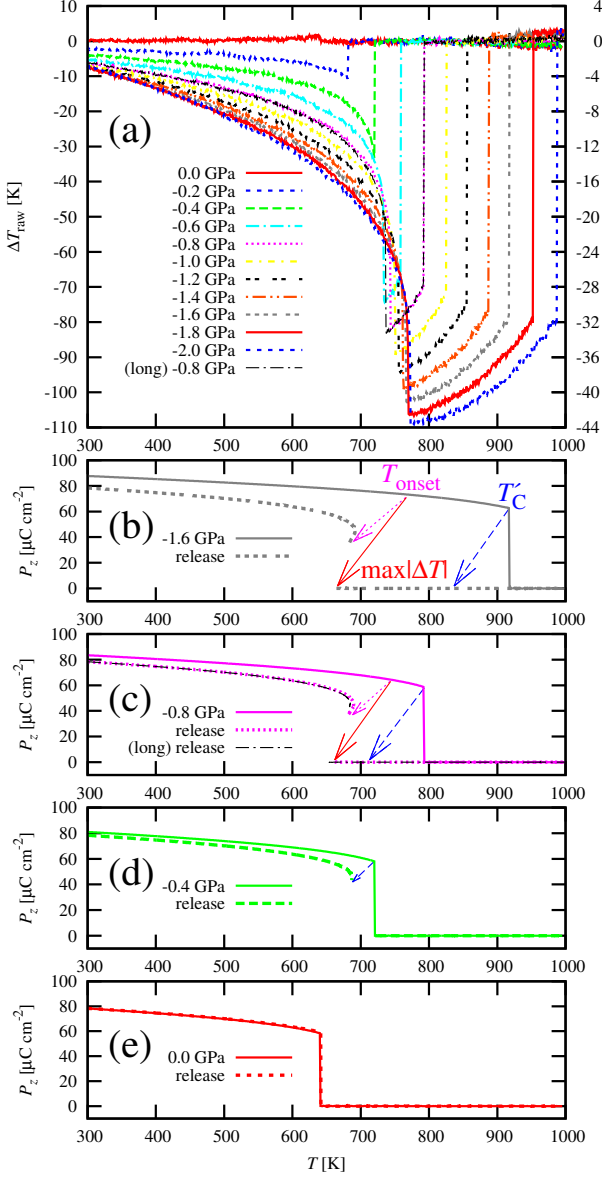


FIG. 2. (Color online) (a) Simulated elastocaloric effect,  $\Delta T$ , in  $\text{PbTiO}_3$  as functions of initial temperature,  $T_{\text{initial}}$ . The applied uniaxial stress ranges from 0 to  $-2.0$  GPa.  $\Delta T$  is scaled from  $\Delta T_{\text{raw}}$  to  $\Delta T_{\text{corrected}}$  by accounting for the reduced degrees of freedom as discussed in Ref. 19. (b) Polarization along the  $z$  axis both before ( $P_z(T_{\text{initial}})$ ) (gray solid line) and after ( $P_z(T_{\text{final}})$ ) (gray intermittent dotted line) the release of load  $-1.6$  GPa. (c)  $P_z(T_{\text{initial}})$  (cyan solid line) and  $P_z(T_{\text{final}})$  (cyan dotted line) of load  $-0.8$  GPa.  $P_z(T_{\text{final}})$  after 990,000 MD time steps (thin black chain line). (d)  $P_z(T_{\text{initial}})$  (green solid line) and  $P_z(T_{\text{final}})$  (green dashed line) of load  $-0.4$  GPa. (e)  $P_z(T_{\text{initial}})$  (green solid line) and  $P_z(T_{\text{final}})$  (green dashed line) of zero load. In (b)–(d), transformations which give  $T_{\text{onset}}$ ,  $\max|\Delta T|$ , and  $T'_C$  are indicated with dotted magenta, solid red and dashed blue arrows, respectively.

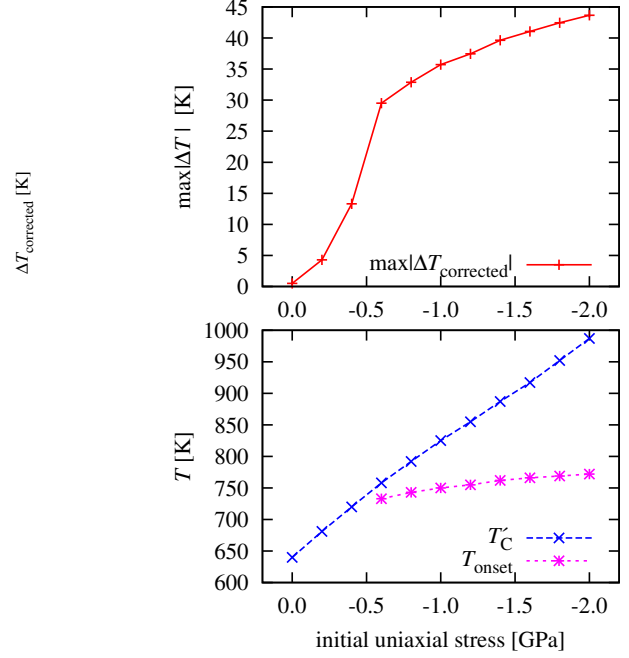


FIG. 3. (Color online) Plots of  $\max|\Delta T_{\text{corrected}}|$ ,  $T_{\text{onset}}$  and  $T'_C$  versus the different initially applied uniaxial tensile stresses. Data are connected with solid red, dotted magenta and dashed blue lines, respectively.

structures. With the elastocaloric effect, domain structures may be formed easier than in the electrocaloric effect where there is no significant  $+z$  nor  $-z$  direction in uniaxial stress, but there is in external electric field. It is suggested that formation of domain structures may cause some degradations in effectiveness in applications of the elastocaloric effect. It should also be noted that when comparing Figs. 2(a) and 4, the onset temperature is constant in switching-on “heating” simulations because the simulations are started from zero stress.

The results presented here can be compared to those presented by Lisenkov *et al.* in Fig. 1(b) of Ref. 11. It should be noted that their  $\Delta T$  is positive because they switched on the uniaxial stress from zero stress. Because of the same reason, their onset initial temperature, which gives  $\max|\Delta T|$ , is always  $T_C$ . We have done the *switching-off* time-dependent MD simulations and found the applied-stress- and equilibration-period-dependence of  $T_{\text{onset}}$  because we believe that hysteretic behavior is important for the cooling application of the elastocaloric effect.

Further, whereas Lisenkov *et al.* report a continuous linear increase of  $\max|\Delta T|$  as stronger stresses are applied and a maximum of approximately  $+35$  K for a tensile load of  $-2.0$  GPa, our results of initial stress dependence of  $\max|\Delta T|$  is not continuous around  $-0.5$  GPa. Our MD simulation for a tensile load of  $-2.0$  GPa results in  $\max|\Delta T_{\text{corrected}}| = |-43|$  K.

Finally, the shape of the two  $\Delta T$  versus  $T$  plots differs in the high temperature regime. Both models have a

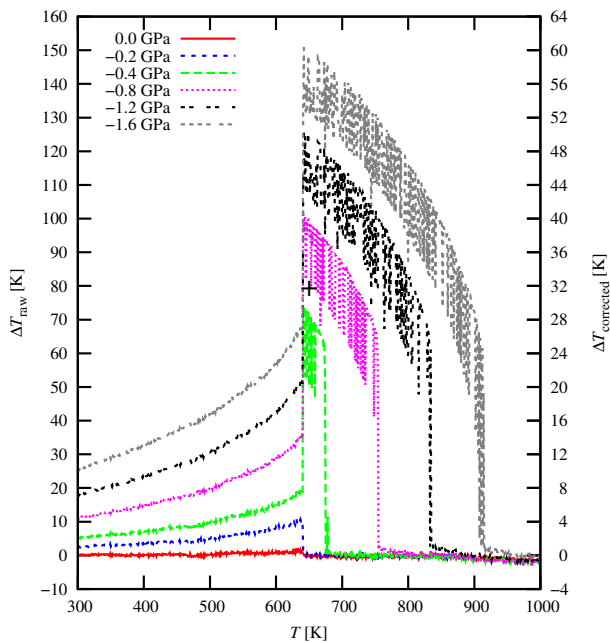


FIG. 4. (Color online) Simulated switching-on elastocaloric effect with positive  $\Delta T$  in  $\text{PbTiO}_3$  as functions of initial temperature,  $T_{\text{initial}}$ . The switched-on uniaxial stress ranges from 0 to  $-1.6$  GPa.  $\Delta T$  is scaled from  $\Delta T_{\text{raw}}$  to  $\Delta T_{\text{corrected}}$ . Zigzag structures in final temperatures are observed. A cross section and a slice of a final state indicated with a “+” mark for a  $-0.8$  GPa simulation are shown in Figs. 5 and 6, respectively.

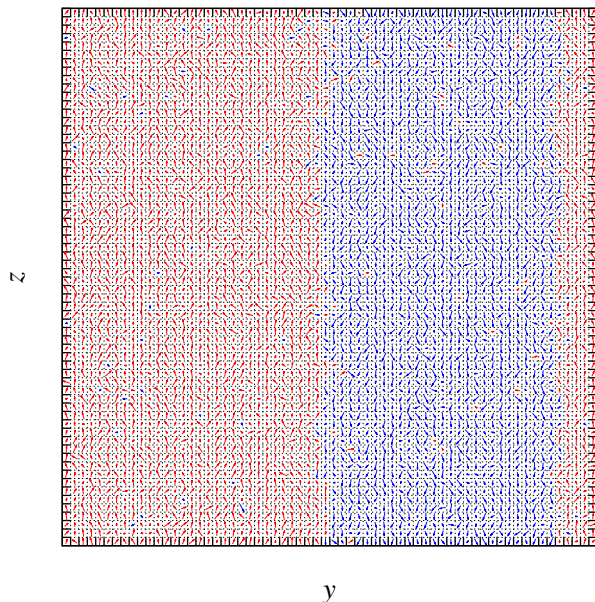


FIG. 5. (Color online) Vertical cross section of a final state indicated with a “+” mark in Fig. 4. Dipole moments of each site are projected onto the  $yz$ -plane and indicated with arrows. The arrows are colored with red or blue if each dipole has  $+z$  or  $-z$  component, respectively.

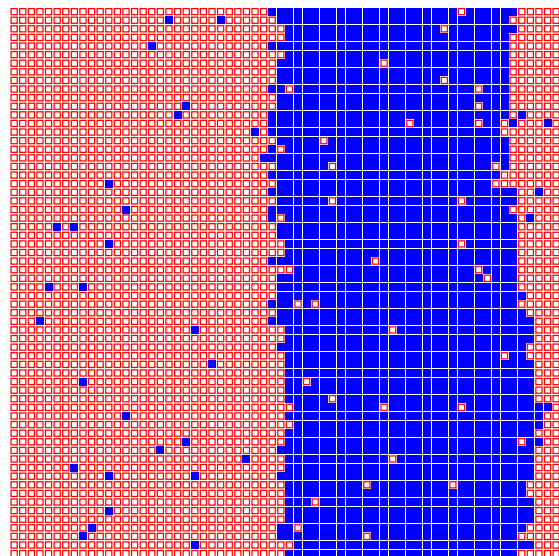


FIG. 6. (Color online) Horizontal slice of a final state indicated with a “+” mark in Fig. 4.  $+z$ -polarized and  $-z$ -polarized sites are denoted by red  $\square$  and blue  $\blacksquare$ , respectively.

$\max|\Delta T|$  that increases with loading, but the results here show a sharper drop in  $|\Delta T|$  at  $T'_C$ , although this difference might be due to differences in the implementations, not the underlying physics. In Fig. 3, it is observed that  $T'_C$  increases linearly with increased loading to a temperature of 1000 K, and presumably above, whereas Ref. 11 states that the elastocaloric response disappears for temperatures above 890 K.

#### IV. SUMMARY

It should be noted that these simulations are very ideal and unrealistic ones. For example, applying such huge tensile uniaxial stresses is difficult and the phase transition of pure  $\text{PbTiO}_3$  would cause cracks in a crystal experimentally. However, these ideal simulations are suggestive to know that, for example, elastocaloric cooling has the largest effect when a ferroelectric to paraelectric phase transition occurs.

In summary, a first-principles based effective Hamiltonian is used within a molecular dynamics simulation to study the elastocaloric effect in  $\text{PbTiO}_3$ . The results find that for modest loading, around  $-0.5$  GPa, a thermal response of around  $-25$  K can be achieved, but for large loads, around  $-2.0$  GPa, the thermal response can be as great as  $-44$  K.

An onset temperature,  $T_{\text{onset}}$ , and termination temperature,  $T'_C$ , are identified as the temperatures bracketing the temperature range where the elastocaloric effect is greatest. The value of  $T'_C$  is found to scale linearly with initial load, while  $T_{\text{onset}}$  has a less steep linearity. Although increasing the initial stress widens the window of temperatures continuously, the initial stress depen-

dence of  $\Delta T$  becomes smaller for stresses stronger than  $-0.5$  GPa.

Formation of domain structures are observed in switching-on “heating” simulations and it is suggested that formation of domain structures may cause some malfunctions in applications of the elastocaloric effect.

The results here are in qualitative agreement with those reported in Ref. 11, which were prepared using an effective Hamiltonian in a Monte Carlo model; however, there are physically significant differences including temperature and applied stress dependence of  $\Delta T$ . There is no easy explanation for these differences, and this might warrant future investigation.

## V. ACKNOWLEDGMENTS

The work of JAB and SPB was supported by the US National Science Foundation (NSF) through grant DMR-1105641. The NSF is thanked for sponsoring JAB’s travel to Tohoku University, which was provided through grant DMR-1037898. The work of TN was supported in part by JSPS KAKENHI Grant Number 25400314. This work was also supported in part by the Strategic Programs for Innovative Research (SPIRE), MEXT, and the Computational Materials Science Initiative (CMSI), Japan. The computational resources were provided by the Center for Computational Materials Science, Institute for Materials Research (CCMS-IMR), Tohoku University. We thank the staff at CCMS-IMR for their constant effort. This research was also conducted using the Fujitsu PRIMEHPC FX10 System (Oakleaf-FX,Oakbridge) in the Information Technology Center, The University of Tokyo.

- 
- <sup>1</sup> G. G. Wiseman and J. K. Kuebler, *Phys. Rev.*, **131**, 2023 (1963).
- <sup>2</sup> J. Scott, *Annu. Rev. Mater. Res.*, **41**, 229 (2011).
- <sup>3</sup> H. Gränicher, *Helv. Phys. Acta*, **29**, 210 (1956).
- <sup>4</sup> E. Hegenbarth, *Cryogenics*, **1**, 242 (1961).
- <sup>5</sup> K. A. Gschneidner Jr, V. K. Pecharsky, and A. O. Tsokol, *Rep. Prog. Phys.*, **68**, 1479 (2005).
- <sup>6</sup> E. Warburg, *Annalen der Physik*, **249**, 141 (1881).
- <sup>7</sup> L. Manosa, D. Gonzalez-Alonso, A. Planes, E. Bonnot, M. Barrio, J.-L. Tamarit, S. Aksoy, and M. Acet, *Nat. Mater.*, **9**, 478 (2010).
- <sup>8</sup> M. Gorev, E. Bogdanov, I. Flerov, and N. Laptash, *J. Phys.: Condens. Matter*, **22**, 185901 (2010).
- <sup>9</sup> P. O. Castillo-Villa, L. Mañosa, A. Planes, D. E. Soto-Parra, J. Sánchez-Llamazares, H. Flores-Zúñiga, and C. Frontera, *J. Appl. Phys.*, **113**, 053506 (2013).
- <sup>10</sup> S. Lisenkov and I. Ponomareva, *Phys. Rev. B*, **86**, 104103 (2012).
- <sup>11</sup> S. Lisenkov, B. K. Mani, C.-M. Chang, J. Almand, and I. Ponomareva, *Phys. Rev. B*, **87**, 224101 (2013).
- <sup>12</sup> J. Cui, Y. Wu, J. Muehlbauer, Y. Hwang, R. Radermacher, S. Fackler, M. Wuttig, and I. Takeuchi, *Appl. Phys. Lett.*, **101** (2012).
- <sup>13</sup> E. Bonnot, R. Romero, L. Mañosa, E. Vives, and A. Planes, *Phys. Rev. Lett.*, **100**, 125901 (2008).
- <sup>14</sup> R. D. King-Smith and D. Vanderbilt, *Phys. Rev. B*, **49**, 5828 (1994).
- <sup>15</sup> W. Zhong, D. Vanderbilt, and K. M. Rabe, *Phys. Rev. B*, **52**, 6301 (1995).
- <sup>16</sup> T. Nishimatsu, U. V. Waghmare, Y. Kawazoe, and D. Vanderbilt, *Phys. Rev. B*, **78**, 104104 (2008).
- <sup>17</sup> U. V. Waghmare and K. M. Rabe, *Phys. Rev. B*, **55**, 6161 (1997).
- <sup>18</sup> T. Nishimatsu, K. Aoyagi, T. Kiguchi, T. J. Konno, Y. Kawazoe, H. Funakubo, A. Kumar, and U. V. Waghmare, *J. Phys. Soc. Jpn.*, **81**, 124702 (2012).
- <sup>19</sup> T. Nishimatsu, J. A. Barr, and S. P. Beckman, *J. Phys. Soc. Jpn.*, **82**, 114605 (2013).